International Journal of Research in Engineering and Science (IJRES)
ISSN (Online): 2320-9364, ISSN (Print): 2320-9356
www.ijres.org Volume 11 Issue 6 ǁ June 2023 ǁ PP. 287-304

Spiral Cyclic and Noncyclic Analytical Solutions of $y'=(ax+b)y^3+cy^2$ for Sciences

H. E. Schulz[1,2], S.A.G. Schulz[3], A.L.A. Simões[4]
[1]*São Carlos School of Engineering, University of São Paulo, São Carlos, 13566-590, Brazil;*
[2]*Samuel Glenn College of Engineering, Auburn University, 21 Spring Instr., Auburn, 36830, USA*
[3]*São Paulo Regional Council of Pharmacy, R. 13453, São Carlos, 13560-648, Brazil*
[4]*Polythecnic School, Federal University of Bahia, Salvador, 40210-630, Brazil*
Corresponding Author: heschulz@sc.usp.br; prof.harryschulz@gmail.com

Abstract
Nonlinear first order equations are common in the several branches of Engineering. The first order differential equation $y'=(ax+b)y^3+cy^2$ is presented linked to particle movements and to chemical reactions. A procedure is proposed to obtain the general solution, which involves the conversion to a second order linear differential equation. The solution is obtained through the roots of the corresponding second order characteristic polynomial, that can be real or complex. It is shown that the solutions of the real roots have a hyperbolic-type behavior (y and x are inversely related, following hyperboles), whereas the behaviors of the solutions of the complex roots are unconventional, presenting a succession of juxtaposed hyperbole-type curves in the linear x, y plot, and which show a spiral component and loops developing in the plane of the "quadrant logx-logy" plot. The solutions are presented here both in parametric form, with x and y related to a parameter s, and in direct form, with y as a function of x. The parametric form is presented because y and x are implicitly related (not explicitly) for the complex roots. The solutions may have implications in the study of physical phenomena governed by nonlinear first order differential equations, and a first discussion on movement of particles subjected to this governing equation is presented.

Keywords: *Particle movement, higher order chemical reactions, functions with sequences of jumps or discontinuities, nonlinear events, nonlinear first order differential equation.*

Date of Submission: 05-06-2023 Date of acceptance: 18-06-2023

I. INTRODUCTION

Nonlinear first order differential equations are commonly found in applied and engineering sciences. Some examples may be cited, like the wave disturbances for stable and unstable parallel flows discussed by Stuart [12], where the proposal of Landau of 1944 was presented as:

$$\frac{d|A|^2}{dt} = k_1|A|^2 + k_2|A|^4 \tag{1}$$

A is the amplitude of the oscillation, t is the time, whereas k_1 and k_2 are coefficients. For constant coefficients, this equation is easily integrable (Bernoulli equation), and the behavior of $|A|^2$ depends on the nature of the coefficients. Also considering oscillations, Dutta and Cooper [3] mentioned the study of Van der Pol of 1926 while commenting the equation

$$\frac{dA}{dt} = \gamma_1 A + \gamma_2|A|^2 A \tag{2}$$

γ_1 and γ_2 are coefficients that may be functions of t meaning respectively, according to the authors, a negative damping, and the main nonlinear factor that damps the solution for large t. Dutta and Cooper [3] continued their comments adding a forcing function Ω to (2), so that:

$$\frac{dA}{dt} = \gamma_1 A + \gamma_2|A|^2 A + \Omega \tag{3}$$

The mentioned authors then conducted their study to a quantum version of the Van der Pol proposal, in

the sense of a quantum harmonic oscillator subjected to dissipative effects. The Van de Pol equation is also studied in its second order form, as shown, for example, by Grasman et al. [5]. When considering another brunch of studies, like the research on nonlinear chemical reactions, also there interesting phenomena described by first order differential equations are generated, like the Belousov–Zhabotinsky (BZ) reaction, which characteristics can be followed by computational simulations, and proven experimentally. The study of Rajans et al. [8], for example, shows interesting experimental aspects of such reactions, while Epstein and Showalter [4] discuss some conceptual aspects of different models on nonlinear chemical dynamics. As known, also problems of movement in astrophysics may lead to first order equations, which nonlinearity imply in searching for adequate possible solutions. For example, Ramntah [9] converted the second order differential Emden-Fowler's equation

$$\frac{d^2u}{dx^2} = -x^{\sigma}u^n \tag{4}$$

into a simplified first order equation of two independent variables τ_0 and τ_1 in the form:

$$a\frac{dB}{d\tau_1} = -\lambda\tau_0^{\sigma}B^n \tag{5}$$

σ, n, and λ are constant parameters (λ=±1); x, τ_0 and τ_1 are independent variables, a is a coefficient depending on τ_0, and u and B are dependent variables. The physical meaning of these variables can be found in Ramntah [9], as well as the procedure to solve (5), for which a separation of variables was used, once two independent variables were proposed. As a general remark related to differential equations, we may remember the comment of Aleksandrov, Kolmogorov, and Lavrent'ev [1], who pointed that "There are not many differential equations with the property that all their solutions can be expressed explicitly in terms of simple functions, as in the case of linear equations with constant coefficients. It is possible to give simple examples of differential equations whose general solutions cannot be expressed by a final number of integral of known functions or as one says, in quadratures".

In the context of nonlinear problems expressed by first order differential equations, the present study considers an equation originated from particle movements subjected to resistive forces and effects of position (variable fields). It is shown that nonlinear chemical reactions of mixed order and subjected to environment time variations (temperature) may also arrive to similar equations.

II. THE EQUATION OBJECT OF THIS STUDY

In the study of particles, the hypothetical problem of a particle ejected in an environment under specific force actions frequently conduces to dead end situations to obtain analytical solutions. The basic reason is our still incomplete knowledge of general solutions of nonlinear equations.

An ejection in perfect vacuum without interferent fields implies in constant velocity. The existence of interactions with fields and particles in a real space induces velocity variations, which evolution depends on the kinds of the interactions. From the macroscopic environment, where the resistance force on a body ejected in some fluid (gas or liquid) is expressed as a power law of the velocity, it may be written that:

$$m\frac{dV}{dt} = -\alpha V^{\tau} \tag{6}$$

V is the velocity of the particle, m is its mass, t is the time, α and τ are respectively the proportionality coefficient and the adopted exponent. To have the velocity in terms of the position x, (6) is multiplied by $dt/dx=V^{-1}$, resulting in:

$$\frac{dV}{dx} = -\frac{\alpha}{m}V^{\tau-1} \tag{7}$$

A composition of two power laws is also commonly used. For liquid media it is common to take the first and the second powers of the velocity, representing respectively laminar and turbulent parcels of the movement

(Schulz et al. [11]). In the present study the composition of two power laws is used, but considering different exponents. The general equation may be written as:

$$\frac{dV}{dx} = -\frac{\alpha}{m}V^{\tau-1} - \frac{\beta}{m}V^{\theta} \tag{8}$$

β and θ are respectively the additional proportionality coefficient and the exponent. Finally, the variation of space conditions along the movement is expressed taking β as a function of the position, or b (x), which may lead to situations without general known solutions:

$$\frac{dV}{dx} = -\frac{\alpha}{m}V^{\tau-1} - \frac{\beta(x)}{m}V^{\theta} \tag{9}$$

The present study was focused on a first-degree polynomial β (x), and the following coefficients and exponents:

$$-\frac{\alpha}{m} = c, \;\; \theta = \tau = 3, \;\; -\frac{\beta(x)}{m} = ax + b \tag{10}$$

a, b and c are constants. Equation (9) assumes the form:

$$\frac{dV}{dx} = cV^2 + (ax + b)V^3 \tag{11}$$

Note that for $\theta = \tau = 1$ into (9), we have a trivial solvable first order equation. For $\theta = \tau = 2$, we have a solvable Bernoulli equation, both cases allowing their detailed description. For $\theta = \tau = 3$ a general solution seems not to be immediately attainable, and the present study shows a way to attain it. This kind of equation can be generated in different fields of study. For example, in the kinetics of nonlinear chemical reactions we are in the context of reactions of mixed orders ("order" used as the value of the exponent of the concentration of the reacting components, as usual in Chemistry). In this case, (12) shows the coexistence of second and third order reactions of the concentration C of the component under study, together with the variation of the environmental conditions along the time t (for example, a continuous linear variation of the temperature of the solution):

$$\frac{dC}{dt} = cC^2 + (at + b)C^3 \tag{12}$$

Equations (11) and (12) illustrate two possibilities of phenomena linked to the same first order non-linear equation. Taking any dependent variable as y and any independent variable as x, the equation under study is given by:

$$\frac{dy}{dx} = (ax + b)y^3 + cy^2 \tag{13}$$

Governing equations can be conveniently nondimensionalized, so that (13) is treated in this study as a nondimensional equation, avoiding the need of introducing specific dimensions.

III. THE SOLUTIONS

3.1 SOLUTION BY INSPECTION

Although not seen as a general way to obtain a solution, this equation has an immediate simple solution obtained by inspection, which is:

$$y = \frac{\Omega}{ax + b} \tag{14a}$$

$$\Omega = -\frac{c}{2} \pm \sqrt{\frac{c^2}{4} - a} \tag{14b}$$

$$y = \frac{-\frac{c}{2} \pm \sqrt{\frac{c^2}{4} - a}}{ax + b} \tag{14c}$$

Fig. 1 shows the two solutions of (14c) using a=b=0.75, and c=2. The very strong superpositions with numerical solutions of (13) using the 4th order Runge-Kutta method show that both procedures (analytical and numerical) lead to the same solution of this equation. If movement of particles is considered, the particles subjected to this equation converge to the discontinuity (±∞ jump) of the function.

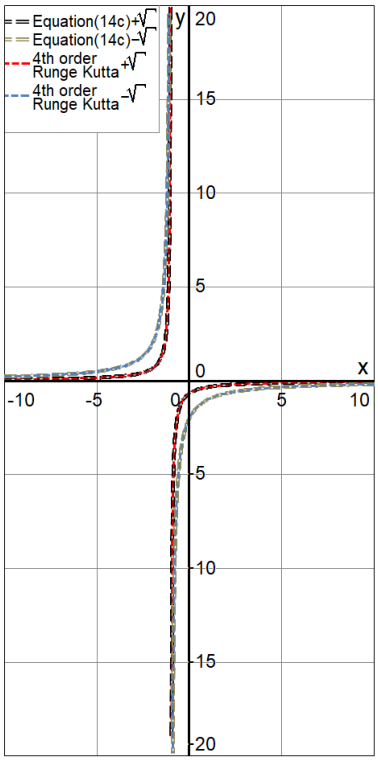

Fig. 1: Noncyclic solutions of equation (14c) for a=b=0.75, c=2. Single ±∞ "jump".

3.2 SOLUTION THROUGH INTEGRATION

By working with an auxiliary second derivative $y=ds/dx$ that inserts the parameter s, we can obtain further solutions of (13), which present additional interesting behaviours. We have then:

$$\frac{d^2s}{dx^2} = (ax + b)\left(\frac{ds}{dx}\right)^3 + c\left(\frac{ds}{dx}\right)^2 \tag{15}$$

The inverse second derivative of the nonlinear equation expressed by (15) is calculated and rearranged to give (see Appendix A):

$$\frac{d^2x}{ds^2} + c\frac{dx}{ds} + ax = -b \tag{16}$$

This is the very basic linear nonhomogeneous 2nd order differential equation with constant coefficients, and has the immediate constant particular solution:

$$x = -\frac{b}{a} \tag{17a}$$

Additionally, its homogeneous solution is given by (see, for example, Boyce and DiPrima, [2]):

$$x = C_1 e^{\left(-\frac{c}{2}+\sqrt{\frac{c^2}{4}-a}\right)s} + C_2 e^{\left(-\frac{c}{2}-\sqrt{\frac{c^2}{4}-a}\right)s} \tag{17b}$$

The complete solution for x as a function of the parameter s is thus given by

$$x = e^{-\frac{c}{2}s}\left[C_1 e^{s\sqrt{\frac{c^2}{4}-a}} + C_2 e^{-s\sqrt{\frac{c^2}{4}-a}}\right] - \frac{b}{a} \tag{17c}$$

The original nonlinear equation was converted into a linear equation with constant coefficients, having a direct general solution, like the equations commented by Aleksandrov, Kolmogorov, and Lavrent'ev [1]. The next steps were directed to obtain y as a function of x, or both variables x and y as a function of the parameter s for specific situations and representations, evidencing different aspects of the original equation. The solution (17c) already shows that different behaviors are obtained for positive and negative radicands of the exponential functions.

3.3 FIRST CASE: POSITIVE RADICAND

Taking firstly $c \neq \pm 2\sqrt{a}$, limited by $-2\sqrt{a} > c > 2\sqrt{a}$, and considering either $C_1 = 0$ or $C_2 = 0$ in (17c), it results:

$$x = Ce^{\left(-\frac{c}{2}\pm\sqrt{\frac{c^2}{4}-a}\right)s} - \frac{b}{a} \tag{18}$$

C is the remaining nonzero integration constant, which may be associated to the + or the – sign of the root. To obtain a solution for y as a function of x, (18) is firstly solved for s leading to:

$$s = \frac{ln\left(\frac{x+\frac{b}{a}}{c}\right)}{\left(-\frac{c}{2}\pm\sqrt{\frac{c^2}{4}-a}\right)} \tag{19}$$

Considering the definition $y = ds/dx$, (19) produces:

$$y = \frac{-\frac{c}{2}\mp\sqrt{\frac{c^2}{4}-a}}{(ax+b)} \tag{20}$$

This is the same solution given by (14c) obtained by inspection, showing that (14c) is related to a more general procedure of integration. It is evidently not necessary to annulate C_1 or C_2 to obtain a solution. For example, maintaining both integration constants and considering $c=\pm 2\sqrt{a}$, (17c) resumes to:

$$x = e^{\mp s\sqrt{a}}[C_1 + C_2] - \frac{b}{a} \tag{21}$$

The parametric variable s is now given by:

$$s = \pm\frac{\sqrt{a}}{a} ln\left(\frac{x + \frac{b}{a}}{C_1 + C_2}\right) \tag{22}$$

From the definition $y=ds/dx$ it results that:

$$y = \pm\frac{\sqrt{a}}{ax + b} \tag{23}$$

Once more, this is the result of (14a, b) for the particular case $c=\pm 2\sqrt{a}$.

Equation (17c) also allows obtaining a more general parametric equation for y, that is, the equation that relates y to s, by applying directly $1/y=dx/ds$ to this equation in the form:

$$\frac{1}{y} = -\frac{c}{2}\left(x + \frac{b}{a}\right) + e^{-\frac{c}{2}s}\sqrt{\frac{c^2}{4} - a}\left[C_1 e^{s\sqrt{\frac{c^2}{4}-a}} - C_2 e^{-s\sqrt{\frac{c^2}{4}-a}}\right] \tag{24}$$

Equations (17c) and (24) have x and y linked to the parameter s, so that graphs of y against x can be easily obtained. As an example, for $a=b=0.75$, $c=2$, and the two pairs of values $C_1=C_2=1.0$ and $C_1=C_2=-1.0$ we have, respectively:

$$x = 2e^{-s}cosh\left[\frac{s}{2}\right] \quad - 1 \tag{25a}$$

$$\frac{1}{y} = -x - 1 + e^{-s}sinh\left[\frac{s}{2}\right] \tag{25b}$$

$$x = -2e^{-s}cosh\left[\frac{s}{2}\right] \quad - 1 \tag{25c}$$

$$\frac{1}{y} = -x - 1 - e^{-s}sinh\left[\frac{s}{2}\right] \tag{25d}$$

The two pairs of values $C_1=C_2=1.0$ and $C_1=C_2=-1.0$ were chosen to produce similar values for positive and negative x, because cosh(s/2) furnishes only positive values. Using the identity $cosh(s/2)+sinh(s/2)=e^{S/2}$ allowed y to be expressed as a function of x, obtaining, as a replacement of (25a-d):

$$y_i = \frac{1}{f_i - \frac{3(1+x)}{2}}; \qquad i = 1, 2, 3. \tag{25e}$$

The index i shows that there are three different possibilities for y_i that depend on f_i, the last given by (see Appendix B):

$$f_1 = \sqrt[3]{\frac{x+1}{4} + \sqrt{\left(\frac{x+1}{4}\right)^2 + \frac{1}{27}}} + \sqrt[3]{\frac{x+1}{4} - \sqrt{\left(\frac{x+1}{4}\right)^2 + \frac{1}{27}}} \tag{25f}$$

$$f_2 = \left(-\frac{1}{2} + i\frac{\sqrt{3}}{2}\right)\sqrt[3]{\frac{x+1}{4} + \sqrt{\left(\frac{x+1}{4}\right)^2 + \frac{1}{27}}} + \left(-\frac{1}{2} - i\frac{\sqrt{3}}{2}\right)\sqrt[3]{\frac{x+1}{4} - \sqrt{\left(\frac{x+1}{4}\right)^2 + \frac{1}{27}}} \tag{25g}$$

$$f_3 = \left(-\frac{1}{2} - i\frac{\sqrt{3}}{2}\right)\sqrt[3]{\frac{x+1}{4} + \sqrt{\left(\frac{x+1}{4}\right)^2 + \frac{1}{27}}} + \left(-\frac{1}{2} + i\frac{\sqrt{3}}{2}\right)\sqrt[3]{\frac{x+1}{4} - \sqrt{\left(\frac{x+1}{4}\right)^2 + \frac{1}{27}}} \tag{25h}$$

Fig. 2 shows the graph generated by the parametric equations expressed by (25a-d), and the curves obtained from (25e, f). For the case of particles, the converging movement of figure 1 is again observed.

Fig. 2 shows that the parametric equations (involving *s*) and the nonparametric equations (expressing *y* as a function of *x*) generate similar results. Figs. 3a-d show the graphs of 25(e-h) taking into account the complex parts of the solutions, which are presented as the third axis in the figures (*y Complex*). As mentioned, these are solutions of (13) for $a=b=0.75$, $c=2$, $C_1=C_2=1$, which were

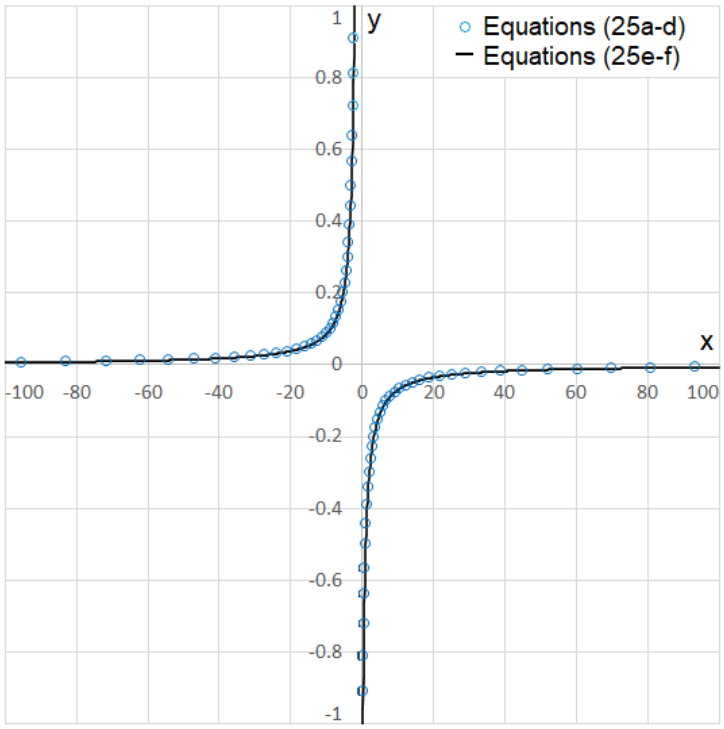

Fig. 2: ±∞ Jump graph of (25a-d) for $C_1=C_2=1.0$ and $C_1=C_2=-1.0$, together with the graph of 25(e-f) for $C_1=C_2=1.0$. *s* was varied between -1.8 and 24.5. The solutions are coincident.

confirmed by inserting (25e-h) into (13), and obtaining the expected identities. The three results have real components. Considering that this set of solutions may physically represent the travel of a particle (from the discussion to obtain (11)), and that the real part of the velocity solution is measurable (observable), Figs. 3a and 3c show that very different velocities could be registered. Figs. 3b and 3d evidence the calculated complex part of the solution (not measurable or observable). The three solutions together show that the real converging $\pm\infty$ "jump" is "bypassed" by the finite complex paths. Evidently, conclusions of physical meanings of the solutions must consider the model itself in relation to the phenomenon it is representing (e.g., particle movements), and the time evolution of the observation, the last being easily obtained through:

$$t_i = \int \left[f_i - \frac{3(1+x)}{2} \right] dx + C_3 \qquad i = 1, 2, 3. \tag{26}$$

C_3 is the integration constant for the time evolution. As already mentioned, the aim of this study was to obtain viable solutions of the proposed nonlinear equation through integrable procedures. Eventual comparisons with other procedures or extensions are beyond the scope of this study. We may cite the possible use of trigonometric identities of higher orders for a generic ω angle, like $cosh^2(\omega) - sinh^2(\omega)=1$, which introduce square roots with double signs in the definition of y (like the condition of Fig. 1). Such details surely enrich debates of this example ($a=b=0.75$, $c=2$, $C_1=C_2=1$) and of other combinations of variables, but, as mentioned, they are beyond of the scope of this study.

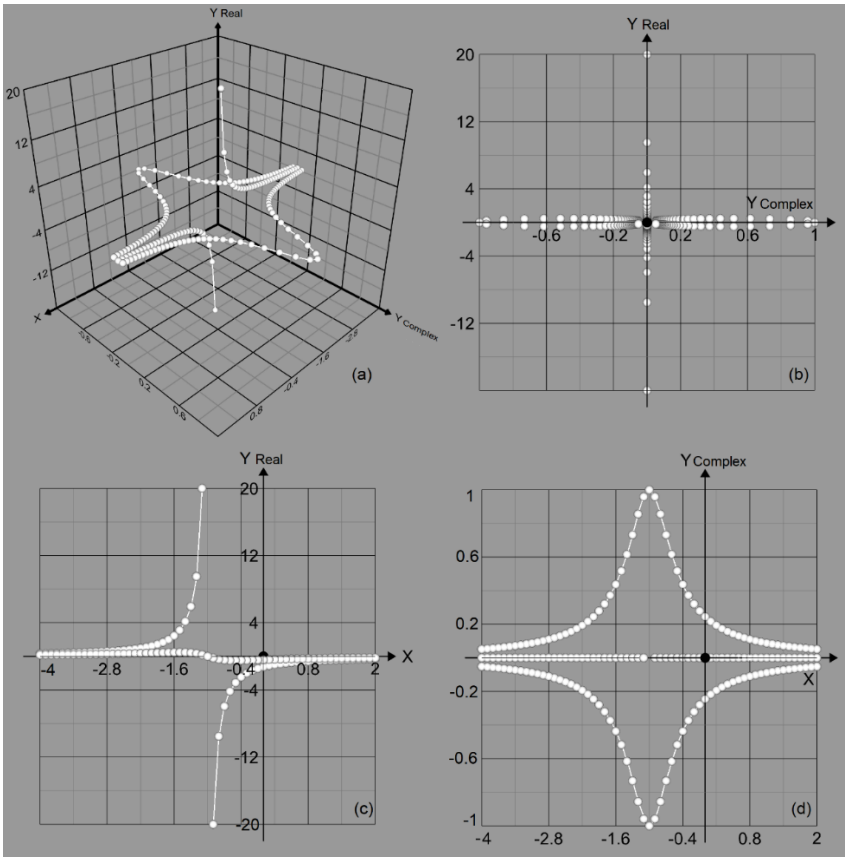

Fig. 3: Complex bypasses to the $\pm\infty$ jump. a) The evolution of solutions (25e-h) in the Real/Complex space, b) The projection of the solutions in the (y Complex, y Real) plane; c) The projection of the solutions in the (x, y Real) plane; d) The projection of the solution in the (x, y Complex) plane.

3.4 SECOND CASE: NEGATIVE RADICAND AND CARTESIAN COORDINATES

A further set of solutions of (13) is obtained for $-2\sqrt{a} < c < 2\sqrt{a}$, and which is developed in the sequence. From (17c) it follows that:

$$x = e^{\frac{-c}{2}s}\left[C_1 e^{is\sqrt{\left|\frac{c^2}{4}-a\right|}} + C_2 e^{-is\sqrt{\left|\frac{c^2}{4}-a\right|}}\right] - \frac{b}{a} \tag{27}$$

Thus, taking the constants C_1 and C_2 that allow using the Euler formula for e^{is} with real coefficients K_1 and K_2, it results:

$$x = e^{\frac{-c}{2}s}\left\{K_1 cos\left[s\left|\frac{c^2}{4}-a\right|^{\frac{1}{2}}\right] + K_2 sin\left[s\left|\frac{c^2}{4}-a\right|^{\frac{1}{2}}\right]\right\} - \frac{b}{a} \tag{28}$$

This choice of coefficients K_1 and K_2 allows working with totally real solutions, not necessary but convenient for this study. Knowing that $1/y=dx/ds$ we have:

$$\frac{1}{y} = -\frac{c}{2}\left(x+\frac{b}{a}\right) + \left|\frac{c^2}{4}-a\right|^{\frac{1}{2}} e^{\frac{-c}{2}s}\left\{K_2 cos\left[s\left|\frac{c^2}{4}-a\right|^{\frac{1}{2}}\right] - K_1 sin\left[s\left|\frac{c^2}{4}-a\right|^{\frac{1}{2}}\right]\right\} \tag{29a}$$

Taking K_1=0 as an example for graph visualization, we have:

$$x = K_2 sin\left[s\left|\frac{c^2}{4}-a\right|^{\frac{1}{2}}\right] e^{\frac{-c}{2}s} - \frac{b}{a} \tag{29b}$$

$$\frac{1}{y} = -\frac{c}{2}\left(x+\frac{b}{a}\right) + K_2\left|\frac{c^2}{4}-a\right|^{\frac{1}{2}} cos\left[s\left|\frac{c^2}{4}-a\right|^{\frac{1}{2}}\right] e^{\frac{-c}{2}s} \tag{29c}$$

Equations (29a, b, c) once more show that it is easy to calculate *y* and *x* having *s* as parameter. In this case, although *s* may be isolated to further directly correlate *x* and *y*, it results in an implicit function between the two variables, as shown in (30) (Appendix C). The resulting sinus function of the natural logarithm may be found in different studies of motion, as shown by Schulz [10] in his work on fluid turbulence.

$$\frac{x+\frac{b}{a}}{\sqrt{\left(x+\frac{b}{a}\right)^2 + \frac{\left[\frac{1}{y}+\frac{c}{2}\left(x+\frac{b}{a}\right)\right]^2}{\left|\frac{c^2}{4}-a\right|}}} = sin\left\{\frac{-1}{c}\left|\frac{c^2}{4}-a\right|^{\frac{1}{2}} ln\left[\frac{1}{K^2}\left[\left(x+\frac{b}{a}\right)^2 + \frac{\left[\frac{1}{y}+\frac{c}{2}\left(x+\frac{b}{a}\right)\right]^2}{\left|\frac{c^2}{4}-a\right|}\right]\right]\right\} \tag{30}$$

Like done for the positive radicand, the analysis of the negative radicand is done with the help of an example, so that the graph visualization is possible. Because of the implicit character of the *x*,*y* equation expressed by (30), the graphs were constructed for the parametric versions (29b) and (29c).

The resulting graphs were built up by calculating *x* and *y* for *s* varying from -100 to 100, and taking K_2=1, *a*=*b*=1.5, and *c*=2. Different values of these variables may lead to different graphs. With the present adopted values of the variables, the graph of the resulting function needed auxiliary visual adjustment operations on the results to allow observing the details of the solutions.

Figs. 4, 5 and 6 show *y* (*x*) plotted in three different ways: i) usual linear plot; ii) applying the 1/21th power to *x* and *y*; iii) "quadrant log-log" plot using (*x*/|*x*|)abs(log(abs(*x*))); (*y*/|*y*|)abs(log(abs(*y*))). The linear plot

generates the impression that all the calculated points fall exactly on the abscissa and the ordinate axes. In fact, this plot hides the cycles that exist in the solution due to the very broad range of values of x in relation to y, and the proximity of the distinct paths followed by the sequence of points, or cycle lines.

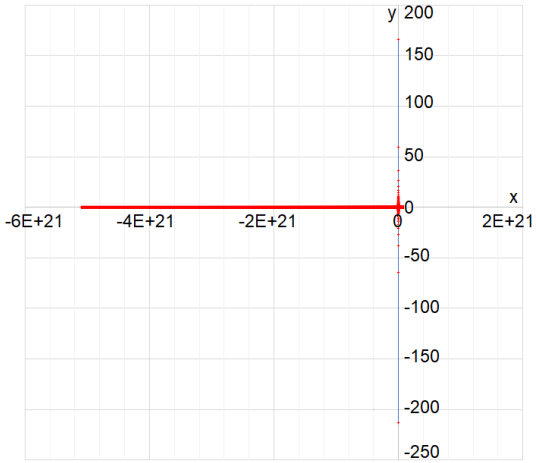

Fig. 4: Linear graph of (x, y) of (29b, c). Red crosses: calculated points. Blue line connects sequential points.

Fig. 4 shows that the order of magnitude of the abscissa x is 10^{21}. To be able to observe details of the evolution of the solution, the $1/21^{th}$ power was applied to both x and y, which showed to be suitable to evidence the cycles generated by this example. The red dots of Fig. 5 are the calculated points, and the blue lines are the connections between successive points. The graph shows a very ordered generation of points. The vertical blue lines show the apparent $+\infty \leftrightarrow -\infty$ "jumps" between sequential points, or local discontinuities, evidenced through vertical spikes. These vertical discontinuities may induce further studies related to their meaning for specific physical cases, and an initial discussion is presented in the next paragraph. Because positive and negative abscissas and ordinates must be calculated, the value of n in the exponent $1/n$ must be and odd number (in the present example, n=21) to allow observing the details of the solution in all quadrants of the 2D plot.

The 1/21 power applied to the results in Fig. 5 distorts the original graph to allow the visualization of the solution, but maintains the relative position among

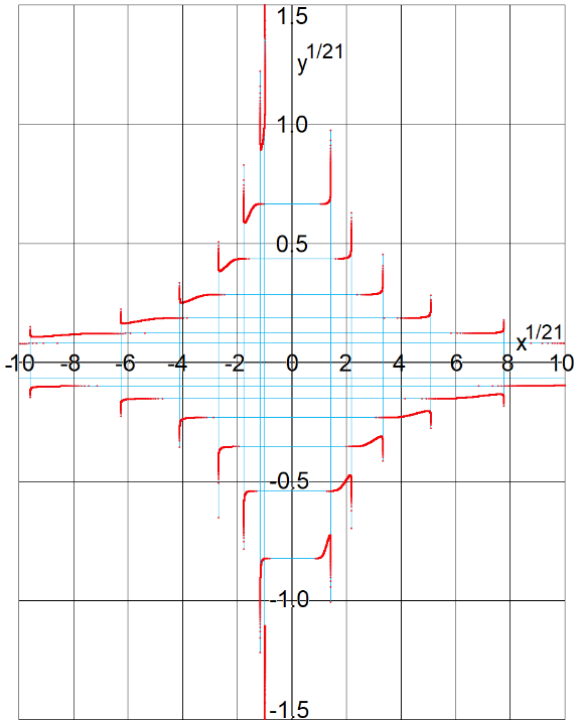

Fig. 5: $x^{1/21}$ and $y^{1/21}$ given by (29b, c) with K_2=1, a=b=1.5, c=2. Red crosses: calculated points. Blue line connects sequential points. A sequence of "jumps" is followed by a particle.

the different calculated points. The evidenced pattern of cycles relating y and x is very interesting, being composed by sequential horizontal quasi-parallel lines with peaks (maxima/minima) in the second and the fourth quadrants of the coordinate system. For the one-dimensional example of a particle ejected in the space (used to generate the governing equation), the mathematical jump between cycles is a characteristic that must be linked to physical possibilities. For example, by attaining one of the x extremes of one of the quasi-horizontal lines of Fig. 5, the velocity (y) increases or decreases (spikes apparently tending to +/-∞) before the particle jumps to the next quasi-horizontal line. This x position is briefly named as x_{jump}. In fact, a "velocity expansion" (sudden acceleration) occurs while the particle is "almost fixed" at x_{jump}, thus it occurs "almost instantly"; and subsequentially the velocity's sign (direction of the movement) changes. It is followed by a "velocity shrinking" (sudden deceleration) to attain the next quasi-horizontal line (or velocity level). Thus, at the jump position x_{jump}, the value of the velocity and its direction are ambiguous in the cycle that promotes the jump. For the other cycles, the same position x_{jump} seems to have stable velocities, although different for each quasi-horizontal line, being positive for the upper lines, and negative for the lower lines. Mathematically, each position x has a number of solutions y that tends to infinity, and the positions x_{jump} seem to allow the jump between different levels of y. If a particle may physically jump between cycles (lines or levels) or not is still a question of debate. The vertical spikes induce to understand that "infinite velocity values" must be attained. If yes, it implies in infinite kinetic energy "to be furnished to or to be generate by" the particle, a not attainable condition. The vertical spikes would then indicate insurmountable energetic barriers. On the other hand, if the infinite velocity is not necessary, then further discussions, which are beyond the scope of this study, may generate interesting results. It must be remembered that the solutions (29a) were taken with real coefficients. Eventual complex coefficients may expand the discussion to consider complex bypasses, like those observed in figure 3 for the positive radicand. The jumping of particles to different "levels of velocity (or levels of kinetic energy)" surpassing energetic barriers is common in the discussions of the atomic shells of electrons, for example, where the energy may involve other concepts (e.g. taking/loosing of photons).

As shown in figure 5, adequate mathematical transformations of the original axes and data allow observing relevant details of the studied equation. Similarly, qualitative different information of the solution can be obtained using the quadrant log-log plot of Fig. 6.

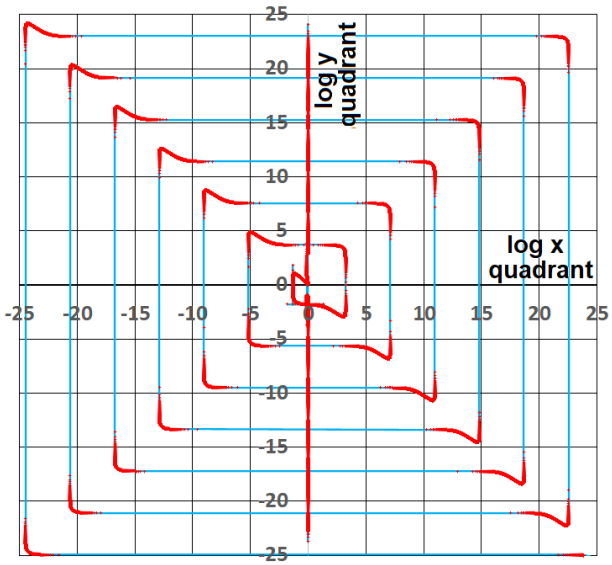

Fig. 6: Quadrant log *y*-log *x* for (29b, c). The cycles of Fig. 5 are evidenced in a spiral form. Red crosses: calculated points. Blue line connects sequential points. Like in figure 5, a sequence of "jumps" is followed by a particle.

The adopted log transformation shows now more evident cycles, which evolve more clearly in an interesting "square spiral" form. Figure 5 shows the superposing spiral, with the jumping positions crossing different quasi-horizontal lines. This crossing of lines is the true characteristic of the solution, but the log transformation ads a further information, which is the arithmetic series observed for the distance to the center of the graph. There are visually constant increments of the distance in the log *x* and log *y* axes, suggesting that the original distance between the cycles (linear graph, Fig. 4) follows a power law (with the vertical jumps evidenced in the $1/21^{th}$ power graph, Fig. 5). Points close to log x=0 and/or log y=0 show vertical and horizontal spikes in the smaller inner cycle. Observable spikes depend on the resolution of the calculations (increments of x and y), and higher resolutions (smaller increments between sequential points) eventually generate spikes in the outer cycles too. The vertical line around log x = 0 is due to $x \rightarrow$-1.0 and $|y| \rightarrow \infty$ for $s \rightarrow \infty$ from equations (26a) and (26b).

The evidencing of the spiral cyclic solution shown in Fig. 6 is very adequate for the present general visualization. It must be noted, however, that this representation shall be used with some care when generating graphs including coordinate points with values both greater and smaller than 1. There is a double trend to ∞ when x and y tend either to 0.0 or to ∞, which may superpose each other, and there is the +/- change of sign around x=1 and y=1. The coordinate points are surely observed in their original quadrants, but the relative position of points with original values between 0.0 and 1.0 is inverted in the quadrant log-log representation. This is clearly the case in the present representation, because the different cycles are now exhibited without crossing lines (in the present resolution), showing a very well-behaved spiral curve. As mentioned, it is clearly adequate to visualize the solution using the quadrant log representation to obtain further information of the solution (like the apparent power law increment of the distance to the center), but the discussion of details of this transformation is not the focus of this study.

3.5 THIRD CASE: NEGATIVE RADICAND WITH RADIAL AND ANGULAR COORDINATES

This third case is an extension of the possibilities of visualization generated by the second case. It does not involve the generation of new solutions, but indicates that the same phenomenon may be analyzed from different points of view. In this sense, (13) is now considered with x initially representing a radial position, and y an angular position. For the plotting in a cartesian plane, the new abscissa and the ordinate are then given, respectively, by:

$$abscissa = [x\,cos(y)]^{1/21} \tag{31a}$$

$$ordinate = [x\,sin(y)]^{1/21} \tag{31b}$$

While in figures 5 and 6 each coordinate was subjected to an independent transformation, we have now a combined transformation of the original coordinates. The exponent 1/21 of (31a, b) once more allows evidencing the details of the solution in graph form. Fig. 7 shows the new presentation of the results, which again assumes a very organized form. The near ordinate positions +1 and -1 stablish the limit between two distinct zones: for -1<ordinate<1 the evolution of the solution occurs mainly along radial lines, whereas for -1>ordinate>1 the evolution occurs mainly along vertical lines. The two horizontal lines y=~arcsin(±1/x) thus characterize boundaries of different behaviors of the equation, an aspect that is not observable in the former plots.

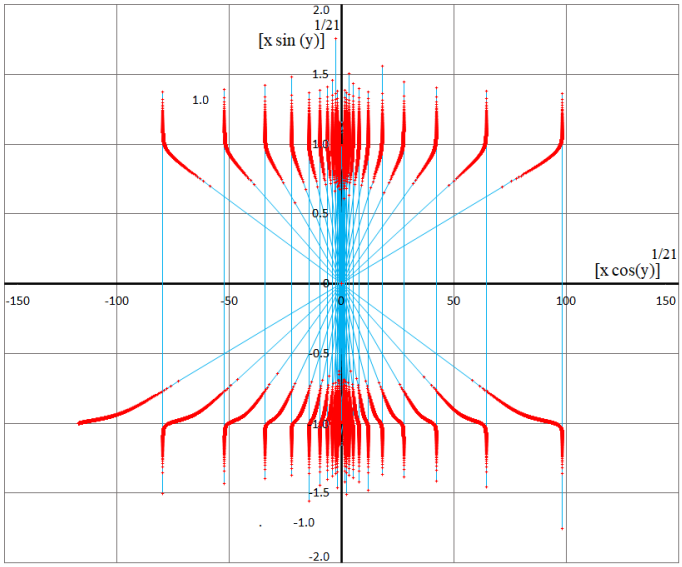

Fig. 7: Combined transformation of coordinates. The solution shows two distinct regions: radial lines and vertical lines. The red crosses are the calculated points and the blue line connect sequential points.

Further, (13) is still considered for radial and angular coordinates, but x is now taking the angular position, and y the radial position. For the plotting in a cartesian plane, the abscissa and the ordinate are given now, respectively, by:

$$abscissa = [y\ cos(x)]^{1/21} \tag{32a}$$

$$ordinate = [y\ sin(x)]^{1/21} \tag{32b}$$

This new combination of the previous coordinates generates the very unregular graph of Fig. 8. Instead of being well-behaved, the graph contains lines (composed by sequential points) that cross each other, and regions where the points are spread resembling graphs of chaotic systems. In these regions the points show evolutions from sparse points to concentrated distributions of points. Although interesting from the point of view of chaotic behavior, the points are evidently calculated following very precise equations. The level of chaotic visual appearance can be at least partially controlled by increasing the number of points of the calculations, that is, increasing the resolution of the graph. In other words, the visual spread of Fig. 8 is partly related to the presently adopted resolution of the graph.

The surprisingly complex behavior of this presentation of the solution (Fig. 8) can be still more evidenced by following the sequence of the generated red points. This was once more accomplished by connecting them sequentially with blue lines, as shown in the maps of Figs. 9 and 10. In this sense, Fig. 9 shows that the calculated points (red crosses) are connected by a large number of horizontal and vertical lines, and also by radial lines more concentrated around the diagonals that form $\pm\pi/4$ angles with the horizontal axis. In the outer part, also some sinuous lines are observed. As already mentioned, it is understood that the resolution of the graphs (the number of calculated points per unit length or per unit area) affects the visual characteristic of the spreading of the points, having thus also influence on the distribution of the blue lines. Figures 8, 9, and 10 present a kind of visual chaos obtained by calculating results of a deterministic equation. This is a usual procedure in studies of chaos, as shown since the very initial studies of May [7] and Feigenbaum [6]. The difference here is that the present results are not used iteratively (like in the mentioned studies of May [7] and Feigenbaum [6]), but each value of the parameter s is used only once to calculate each pair x, y.

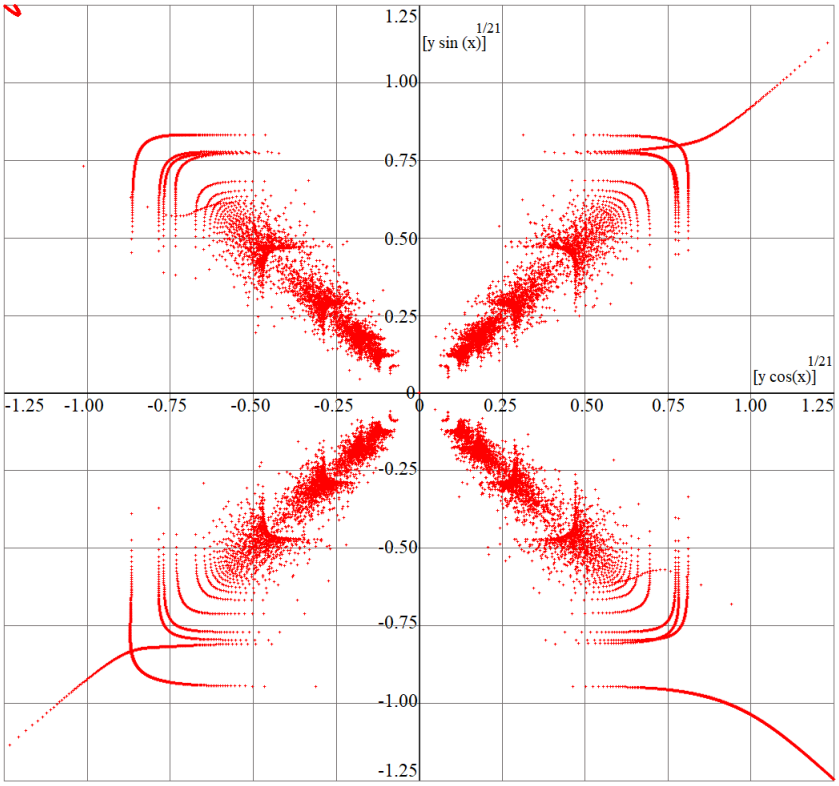

Fig. 8: Combined transformation of coordinates that leads to a chaotic-type representation of the solution. The red crosses are the calculated points.

The difference mentioned in the former paragraph suggests further studies about the characteristics of the present equation and the density of points for its representation. In this sense, comparisons between real systems governed by (13) with collected data (if possible, sparse or dense) and theoretical results would be very welcomed.

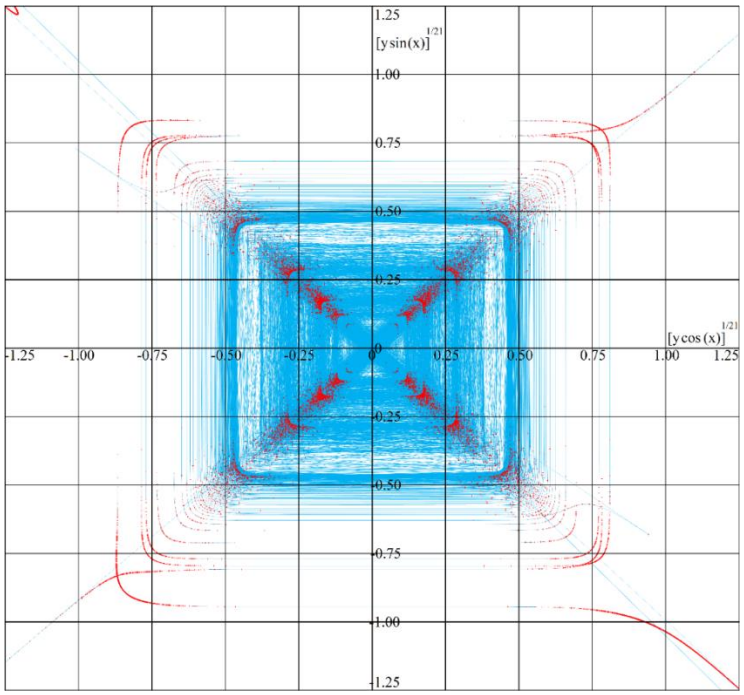

Fig. 9: The same points of Fig. 8 linked sequentially with blue lines, showing concentration of lines along crosses and square forms.

Figure 10 shows an amplification of the second quadrant of Fig. 9. The superposition of lines with different directions is evidenced, once more showing that studies with finer resolutions are welcomed.

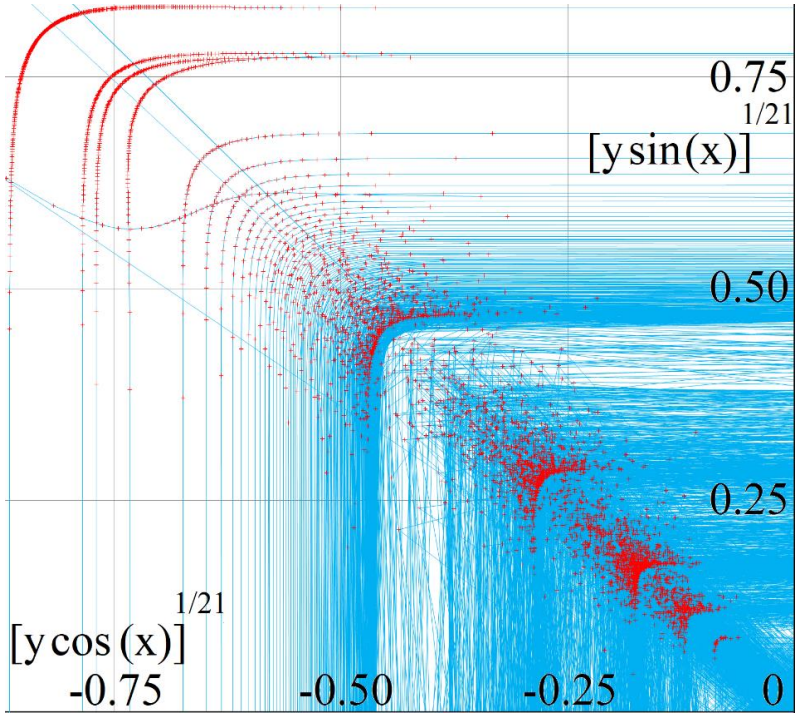

Fig. 10: The amplified second quadrant of the map of figure 9. The crossing of lines is apparent for this resolution and amplification of the calculated points.

IV. CONCLUSIONS

The differential equation $y'=(ax+b)y^3+cy^2$ was converted to a 2nd order differential equation and solved. Considering the one-dimensional particle movement using the velocity of the particle and its position, the examples of this study led to solutions with following characteristics: i) a single ±∞ velocity discontinuity or jump; ii) a ±∞ velocity jump with two complex bypasses iii) cyclic spiral movement containing ±∞ velocity jumps. In the last case, a trend to an infinite number of velocity levels was obtained. Considering the different graph representations, the real-complex space allowed showing the complex bypasses, the 1/21th plot showed details maintaining the relative position of the results, and the quadrant log plot showed the cyclic behavior altering the positions of the results. Further, by applying transformations related to polar variables (radius and angle), a chaotic-type graph was obtained. The solution of the proposed equation was the main focus of this study, but also a discussion about the behavior of the velocity/position of a particle was conducted, showing that the jump between different levels of velocity (kinetic energy) imply in ambiguity of the value and the direction of the velocity in specific positions. These aspects show that the solutions have practical meaning for sciences in general, and for engineering sciences in particular.

REFERENCES

[1] AD Aleksandrov, AN Kolmogorov, MA Lavrent'ev (2013) *Mathematics: its contents, methods and meaning*. Dover Publications, Mineola, New York USA. (reprinted of 1956 original)

[2] WE Boyce, RC DiPrima (2009) *Elementary Differential Equations and Boundary Value Problems*. 9th ed. John Willey & Sons, Inc. USA.

[3] S Dutta, NR Cooper (2019) Critical response of a quantum van der Pol oscillator. *Physical Review Letters*. 123, 250401. doi: 10.1103/PhysRevLett.123.250401.

[4] IR Epstein, K Showalter (1996) Nonlinear chemical dynamics: oscillations, patterns, and chaos. *J. Phys. Chem.* 100(31):13132-13147.

[5] J. Grasman, EJM Veling, GM Willems (1976) Relaxation oscillations governed by a van de Pol equation with periodic forcing term. *SIAM Journal on Applied Mathematics*. 31(4):667-676.

[6] MJ Feigenbaum (1978) Quantitative universality for a class of nonlinear transformations. *Journal of Statistical Physics*. July 19(1):25-52.

[7] RM May (1976) Simple mathematical models with very complicated dynamics. *Nature*. June 216(10): 459-467. doi: 10.1038/261459a0

[8] A Rajans, N Gupte, PC Deshmukh (2020) Non-linear chemical reactions: a comparison between an experiment and a theoretical model. *Resonance*. March 25(3):381-395. doi: https://doi.org/10.1007/s12045-020-0952-8.

[9] RV Ramntah (1971) On a class of nonlinear differential equations of astrophysics. Journal *Of Mathematical Analysis and Applications*. 35, 27-47.

[10] HE Schulz (2022) Differential equation for turbulence power losses and energy spectra based on consolidated empirical results. *Journal of Applied Fluid Mechanics*. 15(4):959-972. https://doi.org/10.47176/jafm.15.04.1041.

[11] HE Schulz, EZ Jakobus, Y Tingchao, IEL Neto, FAS Filho, NA Correa, IM Benites, H Wang (2021) Hydraulics of fluidized cavities in porous matrices: cavity heights and stability for upward water jets. *Journal of Hydraulic Engineering*. 147(10): 04021037 1-14. doi: 10.1061/(ASCE)HY.1943-7900.0001911.

[12] JT Stuart (1960) On the non-linear mechanics of wave disturbances in stable and unstable parallel flows Part 1. The basic behaviour in plane Poiseuille flow. *Journal of Fluid Mechanics*. Nov 9(03):353-370. doi: 10.1017/S002211206000116X.

Acknowledgements

H.E.S., 1st author thanks Prof. Ingo Schulz (Timbó - Blumenau jurisdiction) and Profª. Janka Neuwiem (Kielce - Blumenau jurisdiction) for relevant advices and personal maintenance.

Appendixes

Appendix A: Present method to solve (15).

Equation (15) is rewritten here as (A1):

$$\frac{d^2s}{dx^2} = (ax+b)\left(\frac{ds}{dx}\right)^3 + c\left(\frac{ds}{dx}\right)^2 \tag{A1}$$

The inverse of a second derivative is given by:

$$\frac{d^2s}{dx^2} = -\frac{d^2x}{ds^2}\left(\frac{dx}{ds}\right)^{-3} \tag{A2}$$

Coupling (A1) and A2) leads to:

$$-\frac{d^2s}{dx^2} = (ax+b)\left(\frac{ds}{dx}\right)^3\left(\frac{dx}{ds}\right)^3 + c\left(\frac{ds}{dx}\right)^2\left(\frac{dx}{ds}\right)^3 \tag{A3}$$

By rearranging (A3), the final result is the equation (16) of the text, rewritten below as (A4), and used to solve the problem of this study:

$$\frac{d^2s}{dx^2} + c\frac{dx}{ds} + ax = -b \tag{A4}$$

If higher order differential equations are to be similarly solved through this method, the inverse of a third derivative, for example, is given by

$$\frac{d^3s}{dx^3} = -\frac{d^3x}{ds^3}\left(\frac{dx}{ds}\right)^{-4} + 3\frac{d^2x}{ds^2}\left(\frac{dx}{ds}\right)^{-5} \tag{A5}$$

Appendix B: Obtaining (25e)-(25h):

Equations (25a) and (25b) are rewritten here as (B1) and (B2), respectively:

$$x = 2e^{-s}cosh\left[\frac{s}{2}\right] \quad -1 \tag{B1}$$

$$\frac{1}{y} = -x - 1 + e^{-s}sinh\left[\frac{s}{2}\right] \tag{B2}$$

The identities $cosh(s/2)=(e^{s/2}+e^{-s/2})/2$ and $sinh(s/2)=(e^{s/2}-e^{-s/2})/2$ are applied respectively to (B1) and (B2), producing:

$$\frac{x+1}{2} = \frac{e^{-s/2}+e^{-3s/2}}{2} \tag{B3}$$

$$\frac{1}{y}+(x+1)=\frac{e^{-s/2}-e^{-3s/2}}{2} \tag{B4}$$

Summing (B3) and (B4) results in

$$\frac{1}{y}+\frac{3(x+1)}{2}=e^{-s/2} \tag{B5}$$

Using the definition of $e^{-s/2}$ of (B5) into (B3), performing the cubic operation and rearranging leads to:

$$\frac{1}{y^3}+\frac{1}{y^2}\frac{9(x+1)}{2}+\frac{1}{y}\left[1+\frac{27(x+1)^2}{4}\right]+(x+1)\left[\frac{1}{2}+\frac{27(x+1)^2}{8}\right]=0 \tag{B6}$$

This is a cubic equation for $(1/y)$, which four coefficients a, b, c, d are given by:

$$a=1;\ b=\frac{9(x+1)}{2};\ c=1+\frac{27(x+1)^2}{4};\quad d=(x+1)\left[\frac{1}{2}+\frac{27(x+1)^2}{8}\right] \tag{B7}$$

The auxiliary p and q parameters to express the roots of the cubic equation are:

$$p=\frac{c}{a}-\frac{b^2}{3a^2}=1;\quad q=\frac{d}{a}-\frac{bc}{3a^2}+\frac{2b^2}{27a^3}=-\frac{(x+1)}{2} \tag{B8}$$

The three roots of a cubic equation for $1/y$ are given by:

$$\frac{1}{y_1}=-\frac{b}{3a}+\sqrt[3]{-\frac{q}{2}+\sqrt[2]{\frac{q^2}{4}+\frac{p^3}{27}}}+\sqrt[3]{-\frac{q}{2}-\sqrt[2]{\frac{q^2}{4}+\frac{p^3}{27}}} \tag{B9a}$$

$$\frac{1}{y_2}=-\frac{b}{3a}+\left(-\frac{1}{2}+i\sqrt{\frac{3}{2}}\right)\sqrt[3]{-\frac{q}{2}+\sqrt[2]{\frac{q^2}{4}+\frac{p^3}{27}}}+\left(-\frac{1}{2}-i\sqrt{\frac{3}{2}}\right)\sqrt[3]{-\frac{q}{2}-\sqrt[2]{\frac{q^2}{4}+\frac{p^3}{27}}} \tag{B9b}$$

$$\frac{1}{y_3}=-\frac{b}{3a}+\left(-\frac{1}{2}-i\sqrt{\frac{3}{2}}\right)\sqrt[3]{-\frac{q}{2}+\sqrt[2]{\frac{q^2}{4}+\frac{p^3}{27}}}+\left(-\frac{1}{2}+i\sqrt{\frac{3}{2}}\right)\sqrt[3]{-\frac{q}{2}-\sqrt[2]{\frac{q^2}{4}+\frac{p^3}{27}}} \tag{B9c}$$

Inserting p and q of (B8) into (B9a)-(B9c) produces (25e)-(25h) of the text.

$$\frac{1}{y_1}=-\frac{b}{3a}+\sqrt[3]{\frac{(x+1)}{4}+\sqrt[2]{\frac{(x+1)^2}{16}+\frac{1}{27}}}+\sqrt[3]{\frac{(x+1)}{4}-\sqrt[2]{\frac{(x+1)^2}{16}+\frac{1}{27}}} \tag{B9d}$$

$$\frac{1}{y_2}=-\frac{b}{3a}+\left(-\frac{1}{2}+i\sqrt{\frac{3}{2}}\right)\sqrt[3]{\frac{(x+1)}{4}+\sqrt[2]{\frac{(x+1)^2}{16}+\frac{1}{27}}}+\left(-\frac{1}{2}-i\sqrt{\frac{3}{2}}\right)\sqrt[3]{\frac{(x+1)}{4}-\sqrt[2]{\frac{(x+1)^2}{16}+\frac{1}{27}}} \tag{B9e}$$

$$\frac{1}{y_3}=-\frac{b}{3a}+\left(-\frac{1}{2}-i\sqrt{\frac{3}{2}}\right)\sqrt[3]{\frac{(x+1)}{4}+\sqrt[2]{\frac{(x+1)^2}{16}+\frac{1}{27}}}+\left(-\frac{1}{2}+i\sqrt{\frac{3}{2}}\right)\sqrt[3]{\frac{(x+1)}{4}-\sqrt[2]{\frac{(x+1)^2}{16}+\frac{1}{27}}} \tag{B9f}$$

Appendix C: Obtaining (30):

Equations (29b) and (29c) are rewritten here as (C1) and (C2), respectively:

$$x = K_2 sin\left[s\left|\frac{c^2}{4} - a\right|^{\frac{1}{2}}\right] e^{\frac{-c}{2}s} - \frac{b}{a} \tag{C1}$$

$$\frac{1}{y} = -\frac{c}{2}\left(x + \frac{b}{a}\right) + K_2 \left|\frac{c^2}{4} - a\right|^{\frac{1}{2}} cos\left[s\left|\frac{c^2}{4} - a\right|^{\frac{1}{2}}\right] e^{\frac{-c}{2}s} \tag{C2}$$

Isolating the functions *sin* and *cos* in (C1) and (C2) produce, respectively:

$$sin\left[s\left|\frac{c^2}{4} - a\right|^{\frac{1}{2}}\right] = \frac{\left(x + \frac{b}{a}\right) e^{\frac{c}{2}s}}{K_2} \tag{C3}$$

$$cos\left[s\left|\frac{c^2}{4} - a\right|^{\frac{1}{2}}\right] = \frac{\left[\frac{1}{y} + \frac{c}{2}\left(x + \frac{b}{a}\right)\right] e^{\frac{c}{2}s}}{K_2 \left|\frac{c^2}{4} - a\right|^{\frac{1}{2}}} \tag{C4}$$

Knowing that the sum of the squares of *sin* and *cos* of (C3) and (C4) equals 1, and rearranging, leads to:

$$e^{-\frac{c}{2}s} = \frac{1}{K_2}\sqrt{\left(x + \frac{b}{a}\right)^2 + \frac{\left[\frac{1}{y} + \frac{c}{2}\left(x + \frac{b}{a}\right)\right]^2}{\left|\frac{c^2}{4} - a\right|^{\frac{1}{2}}}} \tag{C5}$$

Solving (C5) for *s* results in:

$$s = -\frac{1}{c} ln\left\{\frac{1}{K^2}\left[\left(x + \frac{b}{a}\right)^2 + \frac{\left[\frac{1}{y} + \frac{c}{2}\left(x + \frac{b}{a}\right)\right]^2}{\left|\frac{c^2}{4} - a\right|^{\frac{1}{2}}}\right]\right\} \tag{C6}$$

Coupling (C1), (C5), and (C6) produces (30) of the text, rewritten here as (C7).

$$\frac{x + \frac{b}{a}}{\sqrt{\left(x + \frac{b}{a}\right)^2 + \frac{\left[\frac{1}{y} + \frac{c}{2}\left(x + \frac{b}{a}\right)\right]^2}{\left|\frac{c^2}{4} - a\right|}}} = sin\left\{\frac{-1}{c}\left|\frac{c^2}{4} - a\right|^{\frac{1}{2}} ln\left[\frac{1}{K^2}\left[\left(x + \frac{b}{a}\right)^2 + \frac{\left[\frac{1}{y} + \frac{c}{2}\left(x + \frac{b}{a}\right)\right]^2}{\left|\frac{c^2}{4} - a\right|}\right]\right]\right\} \tag{C7}$$